Synthesis, Structure, and Magnetic Properties of the Rare-Earth Zintl Compounds $Eu_{14}MnPn_{11}$ and $Eu_{14}InPn_{11}$ (Pn = Sb, Bi)

Julia Y. Chan, Mary E. Wang, Anette Rehr, and Susan M. Kauzlarich*

Department of Chemistry, University of California, Davis, California 95616

David J. Webb

Department of Physics, University of California, Davis, California 95616

Received April 14, 1997. Revised Manuscript Received July 21, 1997[⊗]

New rare-earth transition-metal compounds $Eu_{14}MnPn_{11}$ and $Eu_{14}InPn_{11}$ (Pn = Sb, Bi) have been prepared in quantitative yield from heating stoichiometric amounts of the elements, which are sealed in a welded tantalum tube that is enclosed in a fused silica ampule, at 950−1200 °C. These compounds are isostructural with the Zintl compound $Ca_{14}AlSb_{11}$ and crystallize in the tetragonal space group $I4_1/acd$ ($Z = 8$). Single-crystal X-ray data (143 K) were refined for $Eu_{14}InSb_{11}$ ($a = 17.280$ (5) Å, $c = 23.129$ (8) Å, $R_1 = 4.04\%$, $wR2 = 8.65\%$) and $Eu_{14}MnBi_{11}$ ($a = 17.632$ (4) Å, $c = 23.047(6)$ Å, $R_1 = 4.53\%$, $wR2 = 7.83\%$). The structures of these compounds are compared with $Eu_{14}MnSb_{11}$ and other compounds of this structure type. Magnetization measurements show that $Eu_{14}MnSb_{11}$ and $Eu_{14}MnBi_{11}$ order at approximately 100 and 35 K, respectively. The effective moment in the paramagnetic state for $Eu_{14}MnSb_{11}$ is $\mu_{eff} = 27.0(1)\ \mu_B$ and for $Eu_{14}MnBi_{11}$ is $\mu_{eff} = 27.1(1)\ \mu_B$. $Eu_{14}MnSb_{11}$ saturates with $\mu_{sat} = 102\ \mu_B$ at 5 K whereas $Eu_{14}MnBi_{11}$ does not saturate at 5 K with fields up to 5 T. $Eu_{14}InSb_{11}$ and $Eu_{14}InBi_{11}$ are both paramagnetic at high temperatures with $\mu_{eff} = 30(1)\ \mu_B$ and 30.1(1) μ_B, respectively, and have transitions around 10 K to glassy and antiferromagnetic states, respectively.

Introduction

Since the discovery of $Ca_{14}AlSb_{11}$ by Cordier et al.,[1] a large number of new compounds with this structure has been prepared.[2−12] While most of the effort has focused on the heavier group 15 analogues, $Ca_{14}GaP_{11}$ and $Ba_{14}InP_{11}$ have been recently reported, providing evidence for the existence of a complete family of compounds.[10,11] This structure type fits into the large class of compounds referred to as Zintl compounds.[13−16] In the Zintl−Klemm formalism, there is ionic bonding between the alkaline-earth ions and the main-group anions. The electrons donated from the alkaline-earth atoms are used to fulfill the $8 - N$ rule for the main group atoms.[17] For this structure type, one formula unit consists of 14 A^{2+} cations, 4 Pn^{3-} anions, a MPn_4^{9-} tetrahedron, and a Pn_3^{7-} linear anion.

It has long been recognized that this structure contained an interesting feature of a hypoelectronic Pn_3^{7-} linear anion. Ab initio calculations on $Ca_{14}GaAs_{11}$[18] and recent IR and Raman spectroscopy on $Ba_{14}InP_{11}$[11] are consistent in assigning this unit as a 3-center 4-electron species. In many of the compounds, the central atom in the Pn_3 anion is not symmetrically located.[4,10−12] Because of the asymmetric bond, one might expect that the compounds having this feature may exhibit ferroelectric or other interesting electronic behavior.

The family of compounds that crystallize in this structure type has been enlarged to include the transition metals, Mn and Nb, [2,6,8,9,12,19] as well as the post-transition metals, Zn and Cd.[20] The tetragonal Nb phases, $A_{13}\square NbSb_{11}$ (A = Sr, Eu) are defect variants of the $Ca_{14}AlSb_{11}$ structure with fractional cation vacancies.[19] The defects occur in the substructure of the

* To whom correspondence should be addressed.

[⊗] Abstract published in *Advance ACS Abstracts,* September 1, 1997.

(1) Cordier, G.; Schäfer, H.; Stelter, M. *Z. Anorg. Allg. Chem.* **1984**, *519*, 183.
(2) Kauzlarich, S. M.; Kuromoto, T. Y.; Olmstead, M. M. *J. Am. Chem. Soc.* **1989**, *111*, 8041.
(3) Kuromoto, T. Y.; Kauzlarich, S. M.; Webb, D. J. *Mol. Cryst. Liq. Cryst.* **1990**, *181*, 349.
(4) Kauzlarich, S. M.; Kuromoto, T. Y. *Croat. Chim. Acta* **1991**, *64*, 343.
(5) Kauzlarich, S. M.; Thomas, M. M.; Odink, D. A.; Olmstead, M. M. *J. Am. Chem. Soc.* **1991**, *113*, 7205.
(6) Kuromoto, T. Y.; Kauzlarich, S. M.; Webb, D. J. *Chem. Mater.* **1992**, *4*, 435.
(7) Brock, S. L.; Weston, L. J.; Olmstead, M. M.; Kauzlarich, S. M. *J. Solid State Chem.* **1993**, *107*, 513.
(8) Rehr, A.; Kuromoto, T. Y.; Kauzlarich, S. M.; Del Castillo, J.; Webb, D. J. *Chem. Mater.* **1994**, *6*, 93.
(9) Rehr, A.; Kauzlarich, S. M. *J. Alloys Compounds* **1994**, *207/208*, 424.
(10) Vaughey, J. T.; Corbett, J. D. *Chem. Mater.* **1996**, *8*, 671.
(11) Carrillo-Cabrera, W.; Somer, M.; Peters, K.; von Schnering, H. G. *Chem. Ber.* **1996**, *129*, 1015.
(12) Kauzlarich, S. M. In *Chemistry, Structure, and Bonding of Zintl Phases and Ions*; Kauzlarich, S. M., Ed.; VCH Publishers: New York, 1996; p 245.
(13) Zintl, E. *Angew. Chem.* **1939**, *52*, 1.
(14) Eisenmann, B.; Schäfer, H. *Rev. Inorg. Chem.* **1981**, *3*, 29.
(15) Schäfer, H. *Annu. Rev. Mater. Sci.* **1985**, *15*, 1.
(16) Nesper, R. *Prog. Solid State Chem.* **1990**, *20*, 1.
(17) Kjekshus, A.; Rakke, T. *Struct. Bonding* **1974**, *19*, 45.
(18) Gallup, R. F.; Fong, C. Y.; Kauzlarich, S. M. *Inorg. Chem.* **1992**, *31*, 115.
(19) Vidyasagar, K.; Hönle, W.; von Schnering, H. G. *Z. Anorg. Allg. Chem.* **1996**, *622*, 518.
(20) Young, D. M.; Torardi, C. C.; Olmstead, M. M.; Kauzlarich, S. M. *Chem. Mater.* **1995**, *7*, 93.

S0897-4756(97)00219-6 CCC: $14.00

atoms Sr(3) or Eu(3), with some positions only half-occupied. The $A_{13}\square NbSb_{11}$ compound has only been structurally characterized to date, but the stoichiometry and structure are most consistent with Nb^{5+}.[19] One expects that this compound should be a diamagnetic semiconductor. The Zn and Cd compounds are not stoichiometric and show additional Sb in their structures, although a consistent defect structure was not observed.[20] Temperature dependence of the resistivity of the Zn and Cd compounds have been measured and they are semiconductors.[20]

The $A_{14}MnPn_{11}$ compounds have been shown to have unusual magnetic and electronic properties.[2,3,6,8,9,12,21−23] In these transition-metal Zintl compounds, the metal in the tetrahedron is formally Mn^{III}, a d^4 ion. The temperature-dependent magnetic susceptibility of the arsenic analogues is consistent with this assignment, and the compounds show paramagnetic behavior that can be fit by the Curie−Weiss law.[8] The heavier analogues, Pn = Sb, Bi, show magnetic ordering with $A_{14}MnSb_{11}$ (A = Ca, Sr, Ba)[8] and $A_{14}MnBi_{11}$ (A = Ca, Sr)[6] showing ferromagnetic behavior, and $Ba_{14}MnBi_{11}$ showing antiferromagnetic behavior.[6] Temperature-dependent resistivity measurements suggest that the Sb compounds are semimetals and that the Bi compounds are metallic.[6,8] The magnetic coupling has been attributed to indirect exchange of the localized moments on the Mn mediated by conduction electrons[6,8,22] according to Rudderman−Kittel−Kasuya−Yosida (RKKY) interaction.[24] The highest temperature for magnetic ordering is 65 K for $Ca_{14}MnSb_{11}$.[8]

An extension of this work to the divalent rare-earth analogues has been undertaken. It is expected that the addition of an f-electron ion will lead to interesting electronic and magnetic properties. The single-crystal structure of $Eu_{14}MnSb_{11}$ has been recently reported.[9] This paper presents a more complete study of the $Eu_{14}MnPn_{11}$ phases (Pn = Sb, Bi) and the main-group analogues $Eu_{14}InPn_{11}$. Two new crystal structures are presented, $Eu_{14}InSb_{11}$ and $Eu_{14}MnBi_{11}$. The Sb and Bi compounds were chosen with the idea that the magnetic interactions observed in the alkaline earth analogues might be further enhanced by the presence of an f-electron ion, leading to higher temperature magnetic transitions. These compounds have been characterized by single-crystal and powder X-ray diffraction and temperature- and field-dependent magnetization.

Experimental Section

Synthesis. Eu metal was obtained from Ames Laboratory and cut into small pieces, In shot (J. Matthey, 4 mm shot, 99.99%), Mn pieces (J. Matthey No. 10635, 99.98%), and Sb shot (J. Matthey, 99.99%) were used as received. Bi needles (Anderson Physics, 99.999%) were ground into powder. All materials were handled in an argon atmosphere drybox. All of the $Eu_{14}MPn_{11}$ (M = In, Mn; Pn = Sb, Bi) compounds were prepared by weighing stoichiometric amounts of the elements in a drybox and loading into a clean tantalum tube with a sealed end and subsequently sealing in an argon-filled arc welder. Ta tubes had been cleaned prior to arc welding with 20% HF, 25% HNO_3, and 55% H_2SO_4 solution. The sealed Ta tube was further sealed in a fused silica tube under $^1/_5$ atm of purified argon. In all cases, high yields of polycrystalline pieces were obtained by heating the mixtures to temperatures at 1000 °C for periods between 24 h and 5 days and cooling the reaction to room temperature at rates of 5−60 °C/h. Needle-shaped single crystals along with dendritic crystallites were produced when the reaction temperature was 1250 °C for 3 days. The best method to date for producing crystals from the elements was to heat the reaction mixture in a two-zone furnace with T_{high} = 1000 °C and T_{low} = 950 °C for 10 days. Powder diffraction of all morphologies produced identical powder patterns. All diffraction lines could be indexed according to the correct $Eu_{14}MPn_{11}$ phase. However, $Eu_{14}InBi_{11}$ samples always contain a small amount of Eu_4Bi_3 crystals. Single crystals of $Eu_{14}InBi_{11}$ were not produced by any of the methods described above. All reactions were opened and examined in a nitrogen-filled drybox equipped with a microscope with water levels less than 1 ppm. An interesting aspect of these rare-earth compounds is that they do not appear to be air sensitive. The alkaline earth analogues for the Mn and main group metals are air sensitive and decompose rapidly upon exposure to the atmosphere.

Table 1. Room-Temperature Lattice Parameters

compound	*a* (Å)	*c* (Å)	V (Å^3)
$Eu_{14}InSb_{11}$	17.289(8)	22.77(2)	6807(7)
$Eu_{14}MnSb_{11}$	17.326(7)	22.75(3)	6831(11)
$Eu_{14}InBi_{11}$	17.672(6)	23.11(1)	7218(8)
$Eu_{14}MnBi_{11}$	17.633(3)	23.055(9)	7168(3)

X-ray Powder Diffraction. The products were examined in a drybox under an atmosphere of N_2, then ground up with a mortar and pestle, mixed with approximately 10% silicon and placed between two pieces of cellophane tape. The sample is then transferred to an Enraf Nonius Guinier camera utilizing Cu Kα_1 radiation. Powder diffraction patterns were compared to those calculated from crystal structure data using the program POWDER.[25] Diffraction line positions were read, and 2θ values, *d* spacings, and error bars were obtained from the program GUIN.[26] 2θ values were indexed using the program LATT.[27] The room-temperature lattice parameters are given in Table 1. Powder patterns of the compounds exposed to air for a period of a week were identical with samples that had been handled in the drybox.

Single-Crystal X-ray Diffraction. The tantalum tube was opened in a drybox equipped with a microscope. Metallic looking chunks and dendritic-like highly reflective crystals as well as needles produced from the two-zone method described above were transferred to Exxon Paratone N oil for X-ray structure determination. A suitable crystal ((0.08 × 0.08 × 0.24 mm, $Eu_{14}InSb_{11}$), (0.02 × 0.02 × 0.26 mm, $Eu_{14}MnBi_{11}$)) was mounted on a thin quartz fiber and positioned under the cold stream of N_2 in a R3m/V Siemens diffractometer with a modified Enraf-Nonius low-temperature apparatus (Mo Kα, λ = 0.710 69 Å), and a graphite monochromator. Data collection parameters and crystallographic data are provided in Table 2. The lattice parameters were verified from the axial photographs. No decomposition of the crystal was observed during data collection (inferred from the intensity of the two check reflections). A ψ-scan empirical absorption correction was performed for each structure. The structures were refined using SHELXTL Version 5.03.[28] The largest features in the final difference map for $Eu_{14}InSb_{11}$ and $Eu_{14}MnBi_{11}$ were 3.83

(21) Del Castillo, J.; Webb, D. J.; Kauzlarich, S. M.; Kuromoto, T. Y. *Phys. Rev. B* **1993**, *47*, 4849.
(22) Webb, D. J.; Kuromoto, T. Y.; Kauzlarich, S. M. *J. Magn. Magn. Mater.* **1991**, *98*, 71.
(23) Siemens, D. P.; Del Castillo, J.; Potter, W.; Webb, D. J.; Kuromoto, T. Y.; Kauzlarich, S. M. *Solid State Commun.* **1992**, *84*, 1029.
(24) Kittel, C. *Introduction to Solid State Physics*, 6th ed.; John Wiley & Sons: New York, 1986.
(25) Clark, C. M.; Smith, D. K.; Johnson, G. J. *POWDER*, FORTRAN IV program for calculating X-ray diffraction patterns, Version 5, Department of Geosciences, Pennsylvania State University, University Park, PA, 1973.
(26) Imoto, H. *GUIN*, Fortran Program to calculate 2-theta from film with Si reference lines, Iowa State University, 1979.
(27) Lii, K.; Wang, S.; Garcia, E. *LATT*, Iowa State University, 1985.
(28) Sheldrick, G. M. *SHELXTL, A Program for Crystal Structure Determination*, 5.03, Siemens Analytical X-ray Instruments, Madison, WI, 1994.

Table 2. Crystallographic Parameters

	$Eu_{14}InSb_{11}$	$Eu_{14}MnBi_{11}$
crystal dimension (mm)	0.08 × 0.08 × 0.24	0.02 × 0.02 × 0.26
color and habit	metallic needle	metallic needle
crystal system	tetragonal	tetragonal
temp, K	143	143
space group, Z	$I4_1/acd$, 8	$I4_1/acd$, 8
a , Å	17.280(5)	17.632(4)
c , Å	23.129(8)	23.047(6)
V, Å^3	6906(5)	7165(3)
ρ_{cal} (mg m^{-3})	6.621	8.308
θ range	0° < 2θ < 60°	0° < 2θ < 60°
μ Mo Kα (mm^{-1})	32.74	78.204
transmission coeff range	0.096−0.150	0.097−0.130
scan range ω (deg)	1.0	0.8
scan speed (min^{-1})	4.0	4.0
no. of collected reflections	10955	5175
no. of unique reflections	2530	2628
no. of observed reflections	2138 ($F_o > 4\,\sigma(F)$)	1798 ($F_o > 4\,\sigma(F)$)
no. parameters refined	62	62
$R1$[a]	0.0404	0.0453
$wR2$[b]	0.0865	0.0783

[a] $R = \sum||F_o| - |F_c||/\sum|F_o|$. [b] $wR2 = \sum[w(F_o^2 - F_c^2)^2]/\sum[w(F_o^2)^2]^{1/2}$.

e$^-$/Å^3 and 3.051 e$^-$/Å^3, respectively. Isotropic thermal parameters and anisotropic thermal parameters for each structure are provided as Supporting Information.

Magnetic Susceptibility Measurements. Dc magnetization data were obtained with a Quantum Design MPMS superconducting quantum interference device (SQUID) magnetometer with a 5.5 T superconducting magnet. The data were collected and analyzed with the Magnetic Property Measurement System (MPMS) software supplied by Quantum Design.[29] All samples were prepared in a drybox by loading typically 20−25 mg of powdered sample into a quartz tube designed to provide uniform background. The tube was subsequently sealed under vacuum (1 × 10^{-6} Torr). The temperature-dependent magnetization data were obtained by first measuring the zero-field-cooled (ZFC) magnetization in the field while warming from 5 to 300 K and then measuring magnetization while cooling back to 5 K with the field applied to obtain the field-cooled (FC) data. Field-dependent magnetization data were taken at 5 K with H swept from 0 to 5 T to −5 T and back to 0 T.

Results and Discussion

Structure. Data collection parameters for $Eu_{14}InSb_{11}$ and $Eu_{14}MnBi_{11}$ are shown in Table 2. Table 3 provides the positional parameters and isotropic U's. Table 4 presents selected bond distances and angles for $Eu_{14}MSb_{11}$ (M = Mn, In) and $Eu_{14}MnBi_{11}$. Although single crystals of $Eu_{14}InBi_{11}$ were not obtained, powder X-ray diffraction data are consistent with the $Ca_{14}AlSb_{11}$ structure type. Lattice parameters determined from room-temperature powder X-ray diffraction data are provided in Table 1. All compounds are isostructural to $Ca_{14}AlSb_{11}$,[1] and a perspective view along the c-axis of $Eu_{14}MnSb_{11}$ is shown in Figure 1. This structure type has been described in detail previously.[1−12] For the purposes of this paper, the most important features are the arrangement of the tetrahedra, the Pn_3 units and the surrounding Eu^{2+} cations. Figure 2 shows a perspective down the b-axis with selected Sb and all Eu atoms omitted. The $MnSb_4$ tetrahedra are stacked and translated by $^1/_2$ along the c-axis, alternated with the Sb_3 polyatomic anions.

The Mn tetrahedron is distorted in all compounds reported to date. The variation of compression of the tetrahedron observed in the family of $A_{14}MPn_{11}$ has been attributed to packing constraints, cation size, and general interionic interactions.[10] The compression of the tetrahedron in the Mn compounds has been attributed to Jahn−Teller distortion, since, in all cases, given the same cation and anion, the Mn compounds show the largest distortion.[3,6,8,9] The Eu analogues should be similar in regards to bond distances and angles to the Sr compounds, since the ionic radii of Sr^{2+} and Eu^{2+} are almost the same. (Eu^{2+} has an ionic radius of 1.17 Å, and Sr^{2+} has an ionic radius of 1.18 Å.)[30] Therefore, we can compare the distances and angles of the Eu compounds to the Sr analogues. The Mn is tetrahedrally coordinated by Pn(2) atoms. The Mn tetrahedron in the Eu compounds shows a larger

Table 3. Atomic Coordinates (×10^4) and Equivalent Isotropic Displacement Coefficients (Å^2 × 10^3)

	x	y	z	U_{eq}
		$Eu_{14}InSb_{11}$		
Sb(1)	1332(1)	3832(1)	1250	3(1)
Sb(2)	34(1)	1107(1)	8079(1)	4(1)
Sb(3)	8694(1)	9755(1)	9531(1)	4(1)
Sb(4)	0	2500	1250	6(1)
In	0	2500	8750	3(1)
Eu(1)	−446(1)	−729(1)	8295(1)	4(1)
Eu(2)	−219(1)	1238(1)	49(1)	5(1)
Eu(3)	3547(1)	0	2500	4(1)
Eu(4)	1812(1)	4073(1)	8430(1)	5(1)
		$Eu_{14}MnBi_{11}$		
Bi(1)	1362(1)	3862(1)	1250(0)	10(1)
Bi(2)	50(1)	1099(1)	8125(1)	11(1)
Bi(3)	8685(1)	9731(1)	9530(1)	11(1)
Bi(4)	0	2500	1250	11(1)
Mn	0	2500	8750	9(1)
Eu(1)	−418(1)	−736(1)	8278(1)	11(1)
Eu(2)	−220(1)	1238(1)	4(1)	13(1)
Eu(3)	3553(1)	0	2500	11(1)
Eu(4)	1790(1)	4096(1)	8428(1)	13(1)

Table 4. Selected Bond Distances (Å) and Angles (deg)

	$Eu_{14}InSb_{11}$	$Eu_{14}MnSb_{11}$[a]	$Eu_{14}MnBi_{11}$
Pn(1)−Pn(4)	3.257(1)	3.258(2)	3.397(1)
Pn(1)−Eu(1) × 2	3.336(1)	3.326(2)	3.402(1)
Pn(1)−Eu(2) × 2	3.381(1)	3.421(2)	3.511(1)
Pn(1)−Eu(3)	3.531(1)	3.493(1)	3.514(1)
Pn(1)−Eu(4)	3.316(1)	3.329(2)	3.367(2)
Pn(2)−M × 4	2.865(1)	2.790(2)	2.862(1)
Pn(2)−Eu(1)	3.317(1)	3.313(2)	3.358(2)
Pn(2)−Eu(1′)	3.348(1)	3.355(2)	3.399(1)
Pn(2)−Eu(2)	3.859(1)	3.840(2)	3.954(2)
Pn(2)−Eu(2′)	3.275(1)	3.267(2)	3.317(1)
Pn(2)−Eu(3)	3.387(1)	3.402(2)	3.448(1)
Pn(2)−Eu(4)	3.307(1)	3.282(2)	3.338(1)
Pn(2)−Eu(4′)	3.584(1)	3.522(2)	3.558(1)
Pn(3)−Eu(1)	3.315(1)	3.340(2)	3.389(1)
Pn(3)−Eu(1′)	3.329(1)	3.304(2)	3.370(1)
Pn(3)−Eu(2)	3.395(1)	3.393(2)	3.458(2)
Pn(3)−Eu(2′)	3.292(1)	3.313(2)	3.372(1)
Pn(3)−Eu(3)	3.226(1)	3.252(2)	3.318(1)
Pn(3)−Eu(4)	3.395(1)	3.333(2)	3.388(1)
Pn(3)−Eu(4′)	3.357(1)	3.298(2)	3.350(1)
Pn(3)−Eu(4″)	3.894(1)	3.851(2)	3.914(2)
Pn(4)−Eu(1) × 4	3.327(1)	3.329(2)	3.376(1)
Pn(4)−Eu(2) × 4	3.552(1)	3.581(2)	3.653(1)
Pn(2)−M−Pn(2′)	107.07(2)	105.1(1)	104.69(2)
Pn(2)−M−Pn(2″)	114.39(4)	118.6(1)	119.54(3)
Mn···Mn (Å)		10.352(1)	10.532(1)

[a] Distances and angles from ref 9.

(29) Quantum Design Inc., San Diego, CA 92121.

(30) Shannon, R. D. *Acta Crystallogr.* **1976**, *A32*, 751.

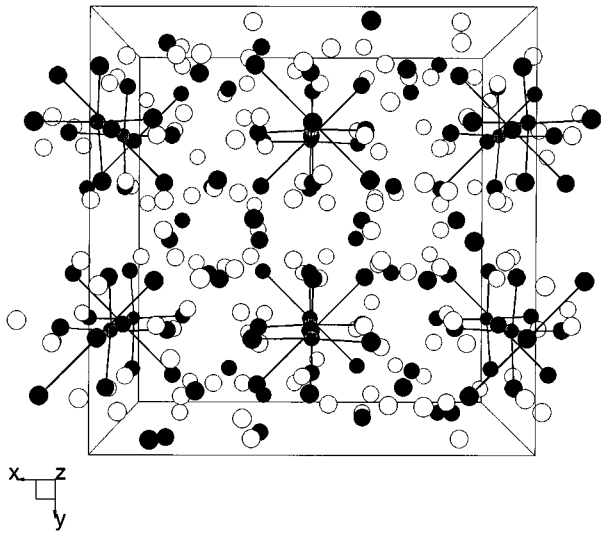

Figure 1. Perspective view of the unit cell down the *c*-axis of $Eu_{14}MnSb_{11}$. The white, gray, and black circles represent Eu, Mn, and Sb, respectively.

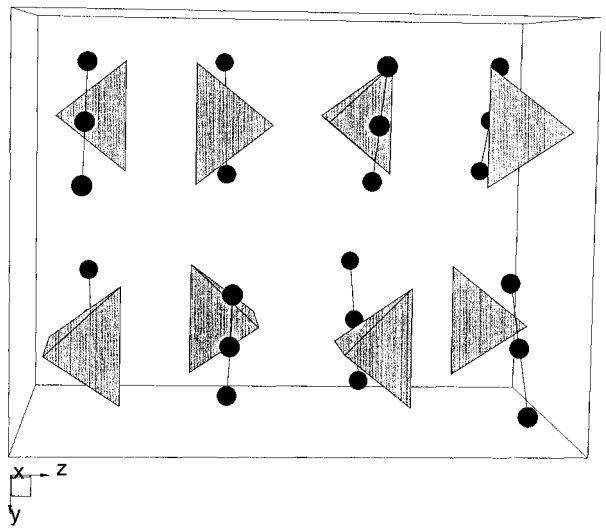

Figure 2. Perspective view of the *b*-axis of $Eu_{14}MnSb_{11}$ with selected Sb anions and $MnSb_4$ tetrahedra shown as polyhedra and Sb_3 units. Eu cations and selected Sb anions omitted for clarity.

distortion than the Sr compounds regardless of pnictogen. The Pn(2)−Mn−Pn(2′) angles are 106.4(1)° and 115.9(1)° for $Sr_{14}MnSb_{11}$[8] while they are 105.1(1)° and 118.6(1)° for $Eu_{14}MnSb_{11}$.[9] The tetrahedral angles for the $Sr_{14}MnBi_{11}$ are 105.0(1)° and 118.7(1)°,[6] whereas the Eu analogue has angles of 104.69(2)° and 119.54(3)°, even more distorted. The MSb_4 tetrahedron in $Eu_{14}InSb_{11}$ is not as distorted as that found in $Eu_{14}MnSb_{11}$, with angles 107.07(2)° and 114.39(4)° for the In compound. If matrix effects[10] were the only influence on the distortion of the tetrahedron, then the In compound is expected to show a larger compression. (The radius for a high spin Mn^{3+} is 0.65 Å and In^{3+} is 0.80 Å.)[30] In addition to the Jahn−Teller distortion observed in these compounds, the Eu cation appears to have an effect that cannot simply be attributed to size.

It is observed that the rare-earth analogues exhibit a larger distortion in the tetrahedron compare with the alkaline-earth analogues. This suggests that the Eu(3) cations interact with the Mn atoms in the tetrahedra through the Pn(2) anions. Figure 3 shows how the Eu(3) atoms link the $[MnPn_4]^{9-}$ tetrahedra and the Pn_3^{7-} polyanion. Pn(2) are the Pn on the corners of the $MnPn_4$ tetrahedra. The Eu(3) atoms represent the exo positions of the Pn_3^{7-} polyanion. With respect to the Pn(2), the Eu(3) atoms form a zigzag chain Mn−Pn(2)−Eu(3) that runs through the structure. Figure 3 shows the anionic octahedral environment of Eu(3) as well as the relationship of the $MnSb_4$ tetrahedra and the Sb_3 linear unit. As shown in this figure, the two Sb(1), the two Sb(2) (corners of the tetrahedron) and two Sb(3) atoms form a Sb_6 octahedron around each Eu(3) atom. The octahedral units bridge the tetrahedra forming the network shown in Figure 3. The Eu(3)−Pn distances are shorter than those observed in the Sr analogues. The A(3)−Sb distances are 3.402(2) Å for A = Eu and 3.452(2) Å for Sr and the A(3)−Bi distances are 3.448(1) Å for A = Eu and 3.502(3) Å for Sr. However, the Mn−Pn(2) distances are consistent with those observed in the Sr compounds. The shortened A−Sb distances are also observed in the $Ho_{11}Ge_{10}$ structure type of $Eu_{11}Sb_{10}$ with Eu−Sb distances ranging from 3.097 to 3.655 Å.[31]

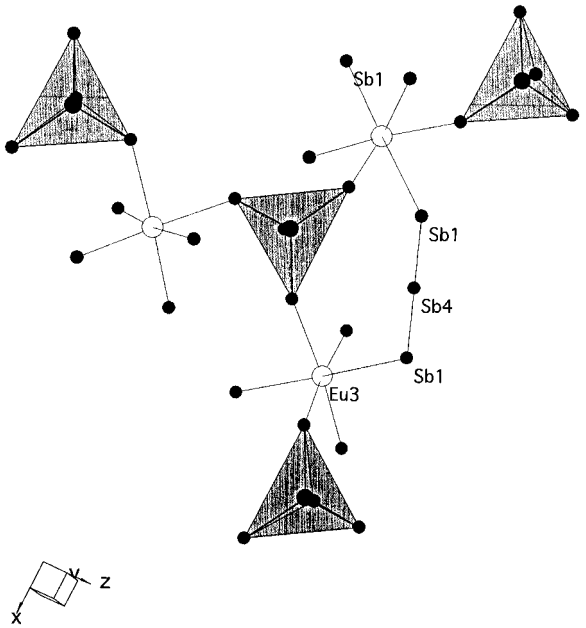

Figure 3. View showing the relationship of the $MnSb_4$ tetrahedra with Eu(3) and the Sb_3 anion. The Mn atoms reside in the center of the shaded polyhedra, Pn(2) are on the corners of the shaded polyhedra, and the white and black circles represent Eu and Sb, respectively.

The Sb−Sb distance in the linear chain is 3.258(2) Å for Mn[9] and 3.257(1) Å for the In compound. These distances are slightly shorter than the Sr analogue (3.310(2) Å).[8] In the Zintl phase Sr_2Sb_3, the Sb−Sb distance ranges from 2.887 to 2.922 Å.[32] Typical single bonds in solid-state compounds are 2.84 Å in the Zintl compound $Ca_{11}InSb_9$[33] to 2.908 Å in elemental Sb.[34] The Bi−Bi distance for $Eu_{14}MnBi_{11}$ (3.397(1) Å) is comparable to the Bi−Bi distance in $Sr_{14}MnBi_{11}$ (3.425(2) Å).[6] The longer Pn−Pn distance observed in the $A_{14}MPn_{11}$

(31) Schmelczer, R.; Schwarzenbach, D.; Hulliger, F. *Z. Naturforsch.* **1979**, *36b*, 1213.
(32) Eisenmann, B. *Z. Naturforsch.* **1979**, *34b*, 1162.
(33) Cordier, G.; Schäfer, H.; Stelter, M. *Z. Naturforsch* **1985**, *40b*, 868.
(34) Barrett, C. S.; Cucka, P.; Haefner, K. *Acta Crystallogr.* **1963**, *16*, 451.

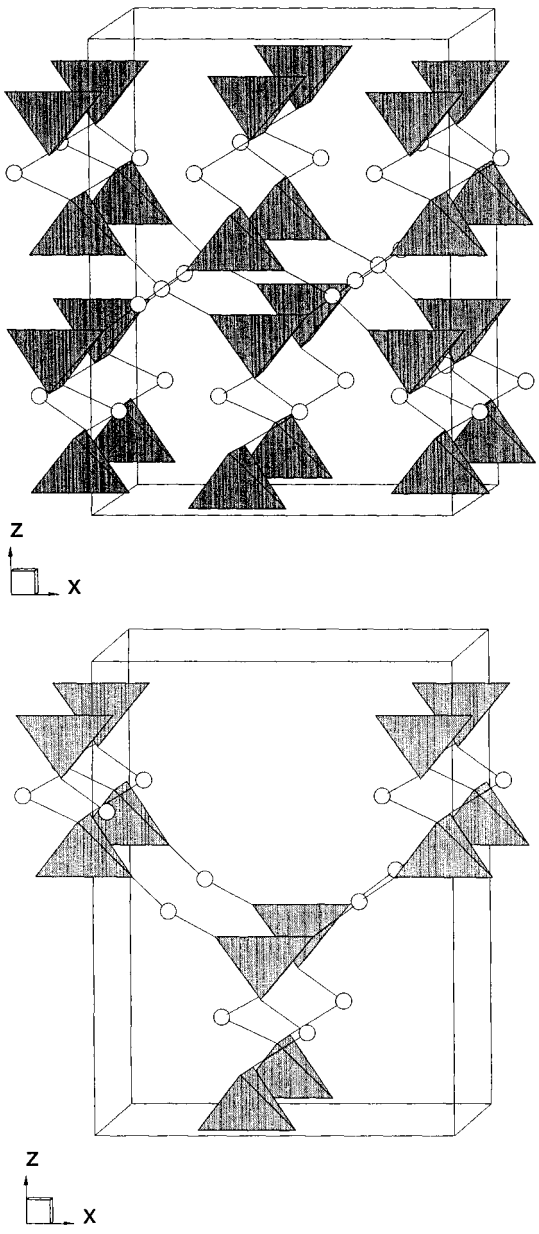

Figure 4. (a, top) View showing the interpenetrating framework formed by the $MnPn_4$ tetrahedra and bridging Eu(3) atoms. (b, bottom) View showing one of the interpenetrating networks formed by [$MnSb_4$] tetrahedra and bridging Eu(3) atoms.

compounds is consistent with the interpretation of the 3-center 4-electron hypervalent bond.[35,36]

It has been shown that the $Ca_{14}AlSb_{11}$ structure is hierarchically related to that of Cu_2O.[11] The connectivity of the tetrahedra within this structure type can be described by two interpenetrating frameworks consisting of [$AlSb_{4/2}$] tetrahedra and [$CaSb_4Sb_{2/2}$] octahedra. Figure 4 shows the two networks which are related by 90° and one of the interpenetrating networks formed by [$MnSb_4$] tetrahedra and the bridging Eu(3) atoms. The six Sb atoms surrounding Eu(3) are omitted for clarity.

Magnetic Properties. Figures 5 and 6 show the magnetic susceptibility and the inverse susceptibility as functions of the temperature (T) for $Eu_{14}InSb_{11}$ and

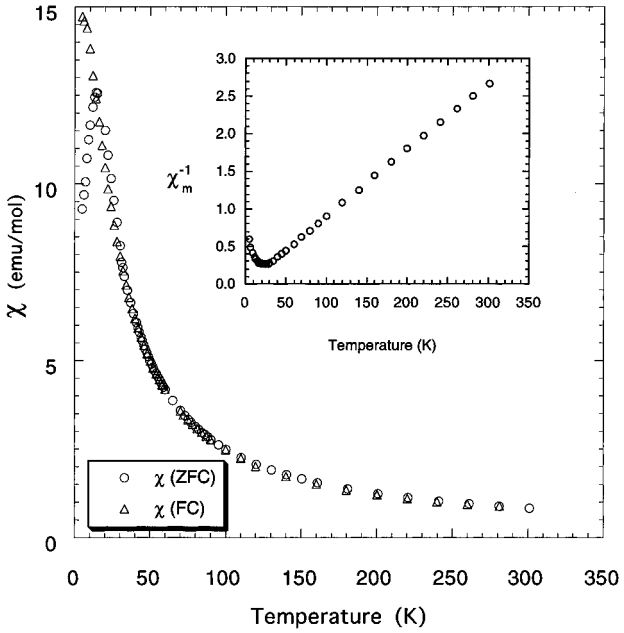

Figure 5. Temperature-dependent magnetic susceptibility and reciprocal susceptibility for $Eu_{14}InSb_{11}$ at 1000 Oe.

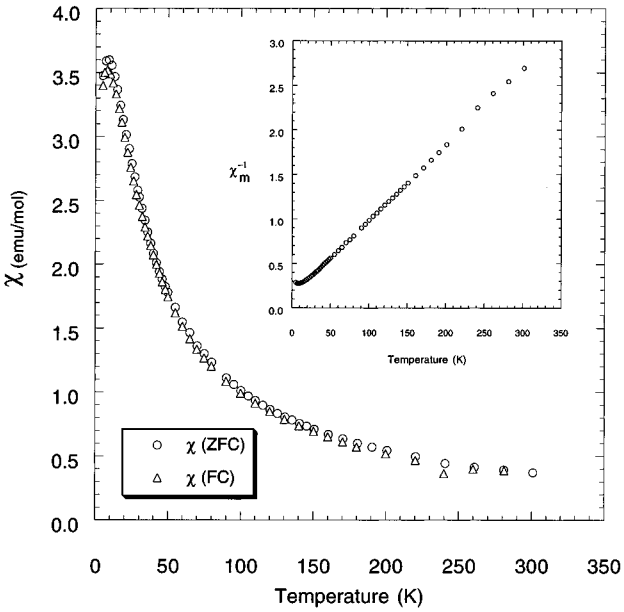

Figure 6. Temperature-dependent magnetic susceptibility and reciprocal susceptibility for $Eu_{14}InBi_{11}$ at 1000 Oe.

Table 5. Magnetic Properties of $Eu_{14}MPn_{11}$ Compounds (M = Mn, In; Pn = Sb, Bi)

	$Eu_{14}InSb_{11}$	$Eu_{14}MnSb_{11}$	$Eu_{14}InBi_{11}$	$Eu_{14}MnBi_{11}$
MW (g/mol)	3581.58	3521.698	4541.11	4481.232
$\chi_0{}^a$ (emu/mol)	0.004(5)	0.09(0)	0.003(2)	0.06(0)
C^a	112(1)	88.9(1)	113.9(5)	85.3(3)
θ^a (K)	0.3(5)	93.55(3)	−14.2(2)	45.1(1)
$\mu_{eff}{}^b$ (μ_B)	30(1)	27.0(1)	30.1(1)	26.1(1)
fit range (K)	50−300	120−300	50−300	150−300
T_c (K)		100		35
μ_s (μ_B)		102		

[a] Obtained from fitting the data to equation $\chi = \chi_0 + C/(T - \theta)$. [b] Using the equation $\mu_{eff} = (8C)^{1/2}$. The theoretical value for the Eu−In compound is 29.9, while that for the Eu−Mn compound is $\mu^2 = 14\,\mu^2_{Eu} + \mu^2_{Mn}$.

$Eu_{14}InBi_{11}$ at 1000 Oe. Table 5 provides the results from fits to the data. These two compounds are magnetically simpler than those containing Mn because the

(35) Pimental, G. C. *J. Chem. Phys.* **1951**, *19*, 446.
(36) Rundle, R. E. *Surv. Prog. Chem.* **1963**, *1*, 81.

magnetic properties are due to the Eu alone. Also, we expect them to be semiconductors or insulators so the magnetic exchange coupling will be short ranged (first and second nearest neighbors) and due to superexchange.

Analysis of the data shows that the high-temperature susceptibility of each of these compounds follows a modified Curie−Weiss law with an effective moment (determined from the Curie constant, C, provided in Table 5) of $\mu_{eff} = 30\ \mu_B$ which is the value one expects for 14 Eu^{2+} ions. The paramagnetic Curie temperature, θ, for the Bi compound is −14.2(2) K so it is not surprising that there is an apparent antiferromagnetic transition around 7 K shown in Figure 6. A more complex magnetic behavior is seen for the Sb compound shown in Figure 5. The θ obtained by a fit of the data to the Curie−Weiss law is nearly zero, and there is no sign of a phase transition in the FC (field-cooled) susceptibility, yet there is still a peak in the ZFC (zero-field-cooled) susceptibility at about 15 K. The 15 K peak in the ZFC data suggests that there are Eu spins which are exchange coupled to their neighbors with total energy of order 15 K. Since θ (which is another measure of the Eu−Eu coupling) is approximately zero, we suggest that there are roughly equal positive and negative Eu−Eu exchange couplings. It is not surprising then that in this rather complicated Eu sublattice there may be a complicated magnetic lattice. This compound might be classified as a spin glass since the dependence of the susceptibility upon thermal history is like that of a spin glass.[37] However, the dependence of the magnetization upon field history, shown in Figure 7, is not what one would expect of a spin glass.[37] In fact, the magnetization at $T = 5$ K is approximately linear, and there is no measureable hysteresis. The magnetic moment of $Eu_{14}InSb_{11}$ does not appear to saturate at 5 T even though the total moment per formula unit is larger than 98 μ_B that one would expect from polarizing all of the Eu moments. Detailed measurements of the magnetic, electronic, and thermal properies of this compound are in progress, and in this paper the low-temperature state will be simply referred to as glassy. Finally, although the low-temperature states of these two materials may differ, the absolute value of the strength of the magnetic coupling in these compounds is not unusual for insulators containing Eu.[38]

Figure 8 shows the magnetic susceptibility and the inverse susceptibility measured at 1000 Oe for $Eu_{14}MnSb_{11}$. It is immediately obvious from the susceptibility that the presence of Mn leads to a magnetic coupling that is ferromagnetic and much larger than the Eu−Eu coupling in compounds made with In. Although the small magnetic signal of one Mn per formula unit cannot be distinguished because of the large magnetic signal of the 14 Eu per formula unit, we attribute the high-temperature ferromagnetic coupling to the Mn−Mn nearest neighbors because of the similarly large couplings observed in other $Ca_{14}AlSb_{11}$-type compounds that do not contain any magnetic ion other than Mn.[6,8] The strong ferromagnetic coupling between Mn spins

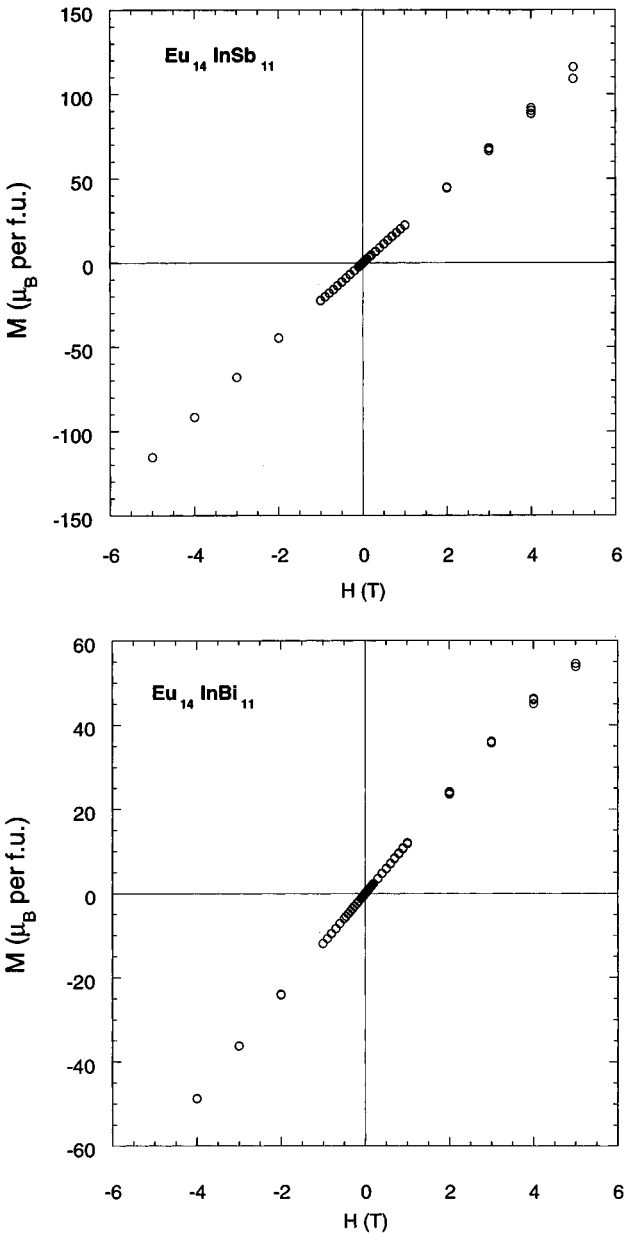

Figure 7. Field-dependent magnetic susceptibility for $Eu_{14}InSb_{11}$ and $Eu_{14}InBi_{11}$ at 5 K.

which are quite far apart (approximately 10 Å) is a distinguishing feature of all of these Mn-containing compounds and provides motivation for continued study. A Curie−Weiss fit to the high-temperature susceptibility shows that the effective moment is smaller than was found for the compounds containing In. This suggests that not all of the Eu spins are ferromagnetically coupled to the Mn spins, and we will see below that this is certainly true.

The magnitude of the susceptibility below 100 K for $Eu_{14}MnSb_{11}$ shown in Figure 8 is almost 2 orders of magnitude larger than that seen in the In compounds. The data show a ferromagnetic transition with a T_c about 100 K. However, the dependence of the magnetization upon T is unusual in two ways. First, for temperatures below T_c the magnetization does not look at all like the mean-field result. The magnetization is growing rapidly as temperature is decreased even well below T_c where the mean field result flattens out.[24] This unusual temperature dependence is likely due to a

(37) Mydosh, J. A. *Spin Glasses: An Experimental Introduction*; Taylor and Francis: London, 1993.
(38) *Handbook of the Physics and Chemistry of Rare Earths*; Gschneidner, K. A., Jr., Eyring, L., Eds.; Elsevier: New York, 1979; Vol. 4.

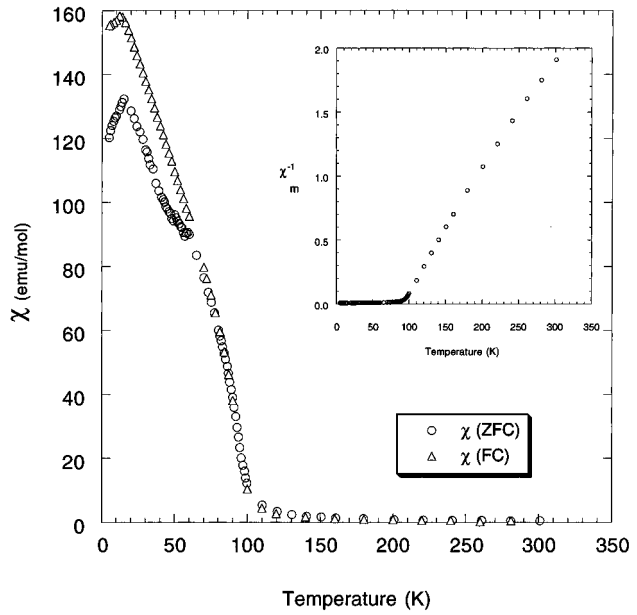

Figure 8. Temperature-dependent magnetic susceptibility and reciprocal susceptibility for $Eu_{14}MnSb_{11}$ at 1000 Oe.

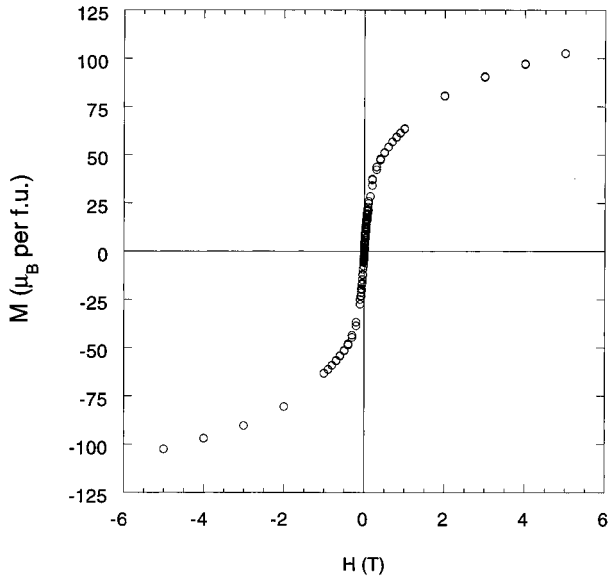

Figure 9. Hysteresis loop for $Eu_{14}MnSb_{11}$ at 5 K.

relatively weak coupling between the Mn spins and some or all of the Eu spins. When the Mn spins order ferromagnetically, they produce a weak molecular field on the set of Eu spins which responds as a paramagnet and produces a magnetization $M(T)$ which is still increasing rapidly well below 0.5 T_c. The second unusual feature is also related to the Eu moments. At about 15 K there is a peak in the susceptibility which we attribute to an ordering on the Eu sublattice. This is presumably due to the same set of Eu−Eu exchange couplings which led to the susceptibility peaks in the In compounds. A low-temperature hysteresis loop of $Eu_{14}MnSb_{11}$ is shown in Figure 9. The loop verifies that the material has a net ferromagnetic moment as we have seen in other Mn compounds in this series and that the coercive field is small.

Figure 10 shows the temperature-dependent magnetic susceptibility of the $Eu_{14}MnBi_{11}$ measured at 1000 Oe. The shape of the magnetic susceptibility suggests that $Eu_{14}MnBi_{11}$ may be an antiferromagnet at low temper-

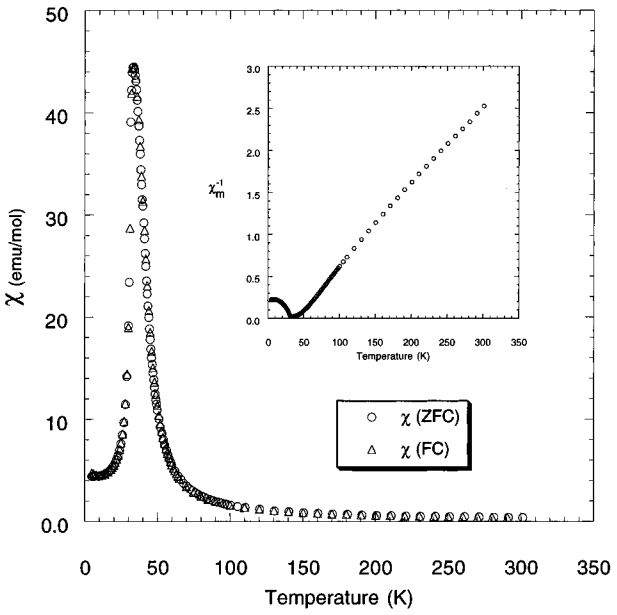

Figure 10. Temperature-dependent magnetic susceptibility and reciprocal susceptibility for $Eu_{14}MnBi_{11}$ at 1000 Oe.

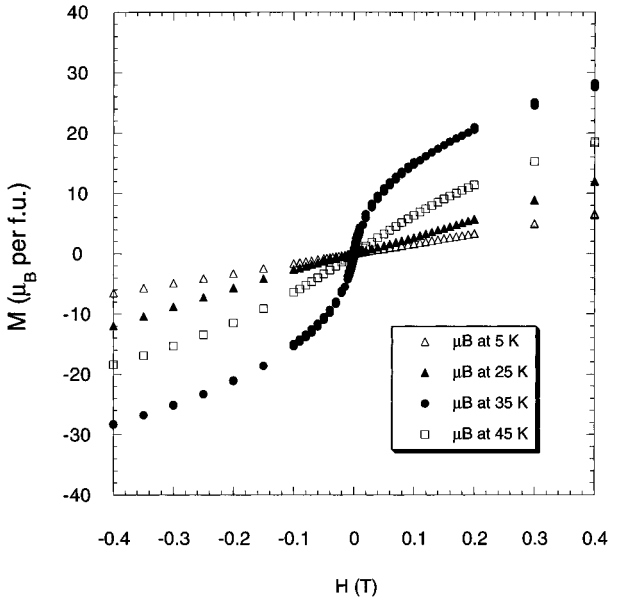

Figure 11. Field-dependent magnetic susceptibility for $Eu_{14}MnBi_{11}$ at various temperatures.

atures. This compound has a behavior roughly similar to that of $Ba_{14}MnBi_{11}$.[22] The positive paramagnetic Curie temperature, θ, suggests that the strongest exchange coupling is ferromagnetic. However, the material appears to order antiferromagnetically. The effects of the ferromagnetic coupling can be seen in the field dependence of the magnetization below the Neel temperature $T_N \sim 35$ K. Figure 11 shows the magnetization as a function of field for several temperatures. For temperatures below T_N there is slight upward curvature of $M(H)$ indicative of a metamagnet[39] where an applied magnetic field can overcome the weak antiferromagnetic coupling and produce a high magnetization state. In fact the magnetization nearly saturates for $T \sim T_N$.

A possible explanation of these two apparently contradictory results comes from an examination of the

(39) Stryjewski, E.; Giordan, N. *Adv. Phys.* **1977**, *26*, 487.

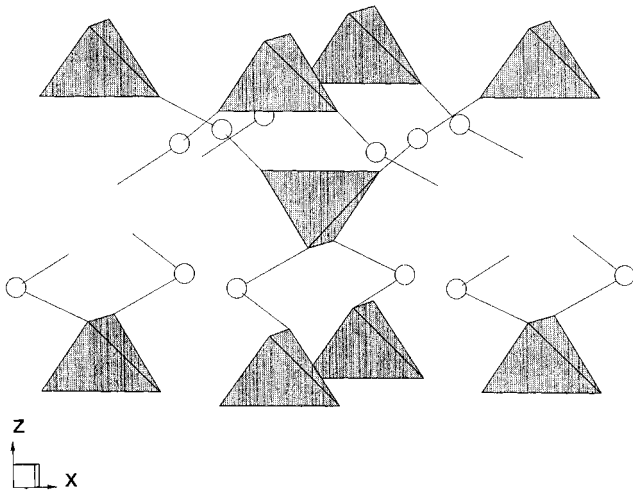

Figure 12. View showing Mn with eight nearest Mn neighbors. The Mn atoms reside in the center of the shaded polyhedra and the white circles are Eu(3).

analysis of the structure by Carrillo-Cabrera et al.[11] The authors identify two distinct Mn sublattices within the $Ca_{14}AlSb_{11}$ structure type which are shown in Figure 4. Each Mn has eight nearest Mn neighbors. The Mn coordination sphere is shown in Figure 12 with equal Mn···Mn distances of 10.352(1) Å for $Eu_{14}MnSb_{11}$. Each Mn is also surrounded by four pnictogen ions so there are four unique directions for each Mn ion along these pnictogen bonds. Because these four directions are oriented toward only four of the eight near-neighbor Mn ions, we suggest that these Mn−Mn neighbors have a different exchange coupling than that of Mn to its other four near neighbors. This division into two sets of exchange couplings results, by the analysis of ref 11, into two separate Mn sublattices with an intrasublattice exchange coupling different than the intersublattice exchange coupling. That is, the two interpenetrating Mn sublattices may have strong ferromagnetic intrasublattice exchange but weak antiferromagnetic intersublattice exchange. This would lead to the apparent discrepancy between a ferromagnetic θ and the observed long-range antiferromagnetic ordering.

Acknowledgment. We thank M. M. Olmstead for assistance with structure determination, J. T. Chang for some sample preparation, P. Klavins for assistance, and R. N. Shelton for use of the magnetometer. We acknowledge Palmer DC (1997) CrystalMaker: A Macintosh Crystal Structures Program Cambridge University Technical Services Ltd., 20 Trumpington Street, Cambridge CB2 1 QA, UK, for structure graphics. Financial support from the National Science Foundation, Division of Materials Research (DMR-9505565) is gratefully acknowledged.

Supporting Information Available: Additional diffraction and refinement data, anisotropic displacement parameters for $Eu_{14}InSb_{11}$ and $Eu_{14}MnBi_{11}$ (3 pages); structure factor tables (12 pages). Ordering information is given on any current masthead page.

CM970219L